Degradation Analysis of Long-term Solid Oxide Fuel Cell Stacks with respect to Chromium Poisoning in La_{0.58}Sr_{0.4}Co_{0.2}Fe_{0.8}O_{3-δ} and La_{0.6}Sr_{0.4}CoO_{3-δ} Cathodes

Qingping Fang, Norbert H. Menzler, and Ludger Blum

Forschungszentrum Jülich GmbH, Institute of Energy and Climate Research (IEK) Wilhelm-Johnen-Straße, 52428 Jülich, Germany

Chromium poisoning as a result of Cr evaporation from the metallic components and the subsequent deposition on the cathode (i.e., air) side is one of the most critical degradation mechanisms in solid oxide fuel cell (SOFC) stacks. Recently, the LSC cathode (i.e., La_{0.6}Sr_{0.4}CoO_{3-δ}) exhibited more promising results in both fuel cell and electrolysis modes than the LSCF (i.e., La_{0.58}Sr_{0.4}Co_{0.2}Fe_{0.8}O_{3-δ}) due to its higher ionic conductivity, despite a relatively larger thermal expansion coefficient (TEC). Furthermore, it has been reported that the oxygen surface exchange kinetics and Sr stability/activity of LSC may imply higher resistance against Cr poisoning by comparison to LSCF. For these reasons, long-term stack operation with both LSCF and LSC cathodes was performed for two different stack designs. The degradation behavior of the stacks with respect to Cr poisoning was analyzed with the support of electrochemical impedance spectroscopy and post-mortem analysis.

Introduction

Although the metallic interconnector of a solid oxide fuel cell (SOFC) or solid oxide electrolysis cell (SOEC) stack does not have any electrochemical function, it is nevertheless a key component that makes the scale-up of the electrical power of solid oxide cells (SOCs) possible. Given the high demands on the material properties at working temperatures (i.e., electrical and thermal conductivities, mechanical and chemical stabilities, thermal expansion compatibility, as well as production and machining costs), possible material candidates are fairly limited. Up until now, chromiaforming alloys, such as Crofer 22 APU, Crofer 22 H, CFY, ITM, and AISI 441 are the most frequently utilized materials for both industrial products and R&D. Due to the nature of chromium evaporation from the metal surface and the subsequent reactions with electrodes (mainly on the air side) inside cells, the chromium poisoning of air electrodes has been a critical degradation mechanism that has been intensively investigated by researchers for more than two decades. The degradation mechanisms of chromium poisoning have been extensively reviewed by different research groups (1-8). Depending on the electrode materials and operating conditions, the deposition of chromium in the electrode, either chemically or electrochemically, tends to dominate the deposition process and, in turn, the degradation behavior. Despite the ongoing debate on the different deposition mechanisms and the dependence of degradation on the operating conditions, degradation relating to chromium evaporation and the poisoning of air electrodes has been effectively reduced by applying a protective coating. More information regarding coatings can be found elsewhere (9-11). Previous long-term stack tests that used the so-called F-design and anode-supported cells (ASCs) have shown that a reproducible low-voltage degradation rate of less than 0.3 %kh⁻¹ can be obtained using state-of-the-art atmospheric plasma-sprayed (APS) MCF coatings (i.e., MnCo_{1.9}Fe_{0.1}O_{3- δ}) and LSCF cathodes (i.e., La_{0.58}Sr_{0.4}Co_{0.2}Fe_{0.8}O_{3- δ}) when operating at 700~750 °C with hydrogen and compressed air under a current density of 0.5 A·cm⁻² and fuel utilization of 40% for at least 35,000 hours (12-14). Similar results could also be obtained with a large stack operated with the internal reforming of LNG at a higher fuel utilization of more than 70% (15). Although ASCs with LSCF cathodes have shown satisfactory resistance against Cr-poisoning with the support of coatings, the LSC cathode (i.e., La_{0.6}Sr_{0.4}CoO_{3- δ}) has drawn increasing attention due to the following characteristics:

- It features higher mixed conductivities and catalytic activity for the oxygen reduction reaction, which also makes it more promising for SOEC operation in view of the delamination of air electrodes.
- Thermodynamic calculations suggest the following stability order for the reaction with Cr-vapors: LSM > LSF > LSCF > LSC (1, 16).
- It has a higher chemical surface exchange coefficient of oxygen and less pronounced degradation due to Cr-poisoning in both dry and humid atmospheres (17, 18).

Compared to LSCF cathodes, the first test of an LSC cathode in an F-design stack already exhibited a possible difference. No chromium was detected anywhere in the cell's cross-section, even though the operating time was only ~600 hours (19). In this study, the electrochemical measurements and post-mortem analysis of the cells with LSCF and LSC electrodes were conducted in two types of stacks, with a focus on different possible degradation behaviors against Cr-poisoning.

Experimental

Different cells were tested in two types of stacks. Detailed information on the cells and stacks is summarized in Table I. Further information on the F-design stacks can be found elsewhere (20). All stacks were tested in a furnace environment. For stacks F1 and F2, the thermocouple for the stack temperature was located in the middle of the interconnector between layers 2 and 3, which was 40 mm deep inside the interconnector. For stacks C1 and C2 (cassette-type stacks), the stack temperature was measured from the top plate, which certainly had a relatively large deviation from the core temperature under load operation. The furnace temperature was kept constant during the constant current operation. However, in order to maintain a stable stack temperature, the furnace temperature was slightly adjusted for stacks F1 and C1 at the end of operation as a result of the increased area-specific resistance (ASR) and increased heat generated. For stack F2, the furnace temperature was also reduced at higher current densities to keep the stack temperature stable throughout the entire operation. The stack's performance was characterized by means of voltage-current (I-V) curves and electrochemical impedance spectroscopy (EIS). The EIS measurements were conducted using a Zahner IM6 Workstation. The frequency range spanned 100 mHz to 100 kHz. The measurements were performed in a near open-circuit condition. However, in order to prevent electrolysis mode from being entered into during the measurements, a DC bias of 5 A was applied with an AC current of 2 A. The distribution function of the relaxation times (DRT) was then calculated using DRTtools (21). Following the operation, samples of the cells were cut by sawing from the repeating unit of each stack for scanning electron microscopy (SEM) characterizations and chemical analysis. For the SEM characterization, a ZEISS ULTRA 55 (Oberkochen, Germany) equipped with an Oxford X-Max (Oxford Instruments— Wiesbaden, Germany) EDX system was used. For the wet chemical analysis, the air electrode with a contact layer was leached with perchloric acid, and the leaching solution was then analyzed by means of inductively coupled plasma - optical emission spectroscopy (ICP-OES) (22).

TABLE I. Information on the tested cells and stacks.

| | F-design | | Cassette design | |
|----------------------------|--|---|--------------------------------|---------------------------------------|
| Stack notation | F1 | F2 | C1 | C2 |
| No. of layers | 4 | 4 | 20 | 10 |
| Active cell area per layer | 80 cm ² | 80 cm ² | 84 cm ² | 84 cm ² |
| Cell supplier | CeramTec half-cell with Jülich cathode | Elcogen | CeramTec | CeramTec |
| Fuel electrode /substrate | Ni/YSZ | Ni/YSZ | Ni/YSZ | Ni/YSZ |
| Electrolyte | 8YSZ (~10 μm) | 8YSZ (~3 μm) | 8YSZ (~10 μm) | 8YSZ (~5 μm) |
| Barrier layer | GDC (4~5 μm) | GDC (<2 μm) | GDC (4~5 μm) | GDC (4~5 μm) |
| Air electrode | LSCF | LSC | LSCF | LSC |
| Contact layer | LSCF | LSCF | perovskite | perovskite |
| Protective coating | APS MCF | APS MCF | WPS MCF* | WPS MCF |
| Interconnector | Crofer 22 APU (2.5 mm) | Crofer 22 APU (2.5 mm) | Crofer 22 APU (0.3 mm) | Crofer 22 APU (0.3 mm) |
| Manifold | Internal | Internal | Internal | Internal |
| Flow mode | Counter-flow | Counter-flow | Co-flow | Co-flow |
| T_furnace | 690~700 °C | 670~700 °C | 730~735 °C | 720 °C |
| T_stack | 725 °C | 725~730 °C | 785 °C | 737 °C |
| Current density | $0.5 \text{ A} \cdot \text{cm}^{-2}$ | $0.5 \sim 1.0 \text{ A} \cdot \text{cm}^{-2}$ | $0.42~\mathrm{A\cdot cm^{-2}}$ | $0.42 \text{ A} \cdot \text{cm}^{-2}$ |
| Fuel utilization | 40% | 40~80% | 70% | 70% |
| Fuel | $100\%~\mathrm{H}_2$ | $100\% \ H_2$ | 50% H ₂ , 50% Ar | 50% H ₂ , 50% Ar |
| Operating time under load | ~6,200 h | ~12,300 h | ~5,000 h | ~11,000 h |

^{(*12} layers were coated with MCF by wet powder spraying, whereas the other 8 were not coated).

Results and discussion

Stacks in the F-design

Figure 1 shows the voltage evolutions of the two F-design stacks, F1 and F2. The following aspects must be considered in the analysis:

- Stack F1 was tested with a constant current density of 0.5 A·cm⁻² and fuel utilization of 40%. Compressed air and dry hydrogen were used for the first 4,500 h of operation (operating period I). After that, compressed air was replaced

by ambient air (operating period II with an active carbon filter and period III without one). In this study, only stack F1 was partially tested with ambient air. All of the other stacks were tested using compressed air only. As can be seen from the voltage evolution and EIS measurements (not shown), no increased degradation was observed with ambient air over more than 1,000 h of operation, before the stack was cooled down for the replacement of the gas valves in the hydrogen pipeline. The calculated voltage degradation rate from 500 h to 6,000 h was 0.38%kh⁻¹.

- Stack F2 began with the same operating parameters as stack F1. Due to the lower ASR resulting from the thinner electrolyte and LSC electrode, stack F2 exhibited much better performance. After 2,100 h of stable operation, the fuel utilization was increased from 40% to 80% stepwise (operating periods I–IV). There was also no essential change in the voltage degradation rate, which had an average value of 0.30%kh⁻¹. Then, the current density was increased to 0.75 A·cm⁻² and 1 A·cm⁻² (periods V and VI), respectively, at a constant fuel utilization of 80%. As noted previously, the furnace temperature was reduced from 700 °C to 670 °C in order to keep the temperature in the middle of the stack stable. In consequence, the temperature gradients within the top and bottom layers increased, which may lead to changes in the contact situation between the cells and interconnector. This could be the reason for the faster observed degradation of layer 1 during operating period VI, which can be confirmed by the typical "bathtub" characteristic of I-V curves (23). Such a phenomenon was also observed and analyzed in previous stack tests in the case of an inhomogeneous contact situation within the stack (24). The calculated average voltage degradation rate of periods V and VI without layer 1 was 0.63%kh⁻¹. With the doubled current density, the voltage degradation rate at 1 A·cm⁻² was roughly twice that at 0.5 A·cm⁻², which indicates a similar degradation rate of ASR over the complete testing period. These results and conclusions also correspond well to the previous ones (24).
- Both stacks F1 and F2 were simultaneously cooled down for the replacement of the gas valves. After restarting, both showed extremely high degradation rates. An EIS/DRT analysis could confirm that the stacks were not degraded due to the thermal cycle. However, the fuel electrodes (especially their electrocatalytic activity) degraded during further operation. As the focus of this study is the possible differences in degradation between the LSCF and LSC air electrodes, analysis of the fuel electrodes exceeds its scope, and will therefore not be discussed further.

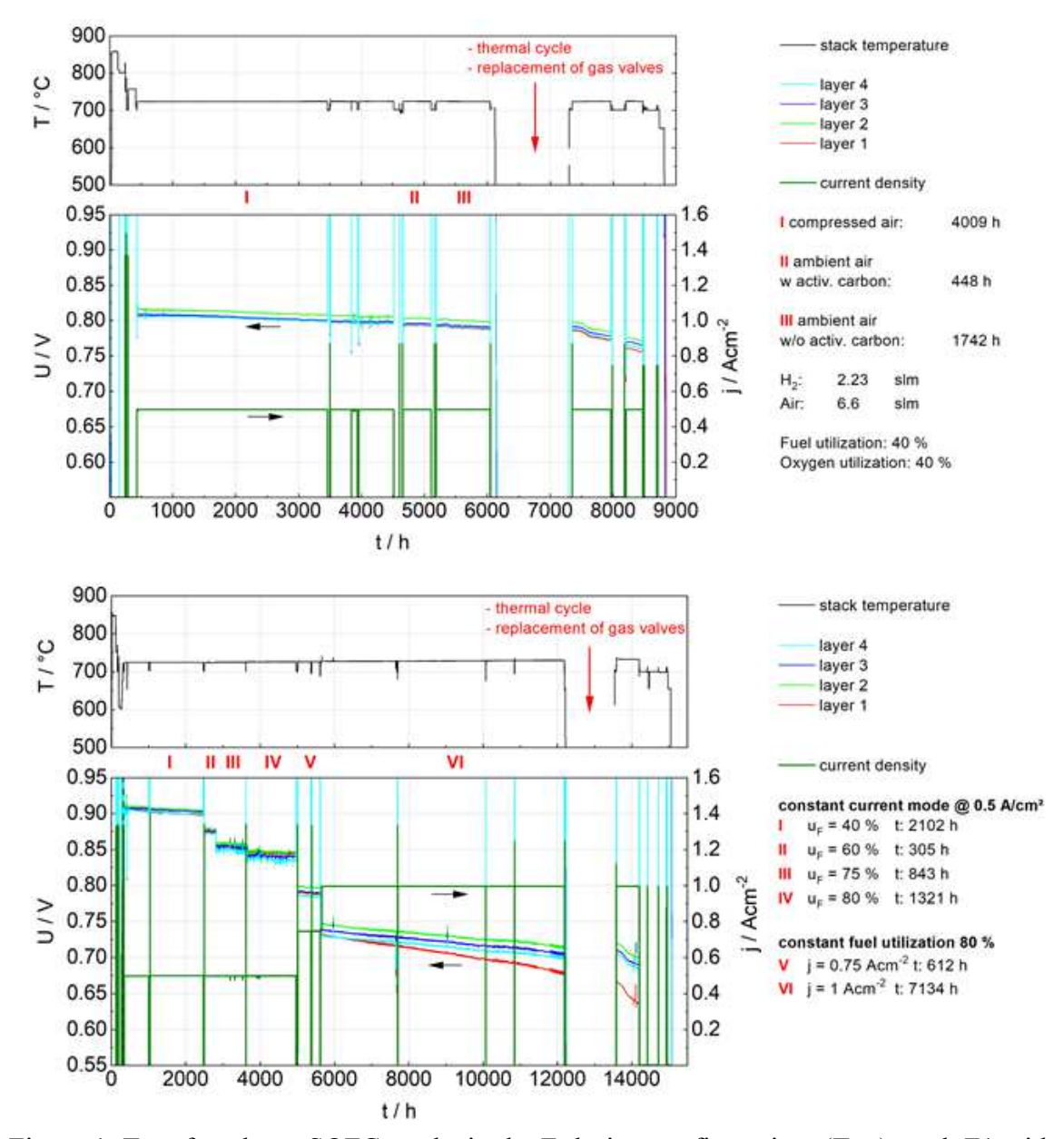


Figure 1. Two four-layer SOFC stacks in the F-design configuration. (Top) stack F1 with the LSCF air electrode; and (bottom) stack F2 with the LSC air electrode.

Figure 2 displays some Nyquist plots and a DRT analysis of layer 2 of each stack. Note that the testing periods of the measurements are different in each stack. Therefore, a direct comparison between the stacks is not recommended. The main takeaway here is that the degradation of both stacks during the selected periods was not dominated by the air electrode, which according to the previous studies is characterized by the second peak close to 100 Hz in the DRT plot (25-27). However, it must be kept in mind that this peak is generally overlapped with the secondary peak of the diffusion process in the substrate (especially with dry gas), which makes the identification of the air electrode polarization difficult, if the degradation itself is small. In both stacks, the EIS measurements were mostly performed using dry hydrogen because of the unstable steam supply of the test benches.

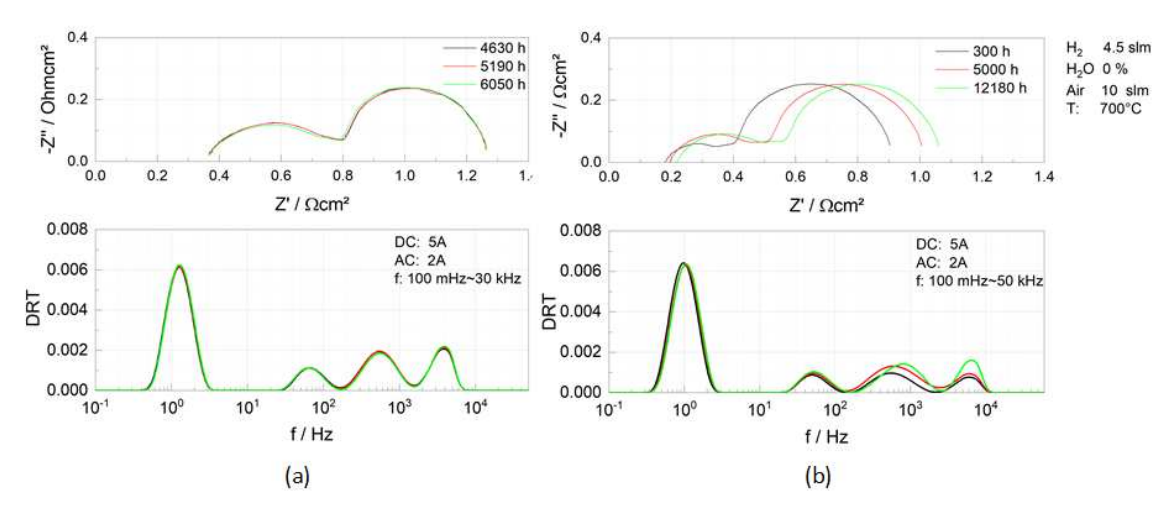


Figure 2. EIS and DRT analysis of an F-design (a) stack F1 with an LSCF; and (b) stack F2 with an LSC. From each stack, only layer 2 is plotted. (Note the different testing periods).

The amounts of chromium incorporated into the air electrodes following operation were characterized by means of a wet chemical analysis with ICP-OES. Two samples at the air inlet and outlet from two layers of each stack were measured. The total quantities obtained in the electrode area for stack F1 (LSCF) and F2 (LSC) were 33-105 µg·cm⁻² (mean value: 61 μg·cm⁻²) and 13-26 μg·cm⁻² (mean value: 19 μg·cm⁻²), respectively. A comparison of the Cr-amount with the previously reported results of the F-design stacks is shown in Table II. Although stack F1 featured the highest amount of chromium among the selected stacks, except for the one with 100,000 h of operation, these values are still typical for this design, materials, and these operating conditions. A clear correlation of the Cr-amount to ambient air cannot be drawn yet. Compared to stack F1, stack F2 with the LSC electrode exhibited a very low Cr-content, and nearly doubled its operating time. However, it's also too early to conclude that the LSC electrode has a higher tolerance against the Cr-deposition, as the lower Cr-content was also observed in the stack with the LSCF electrode and longer operating time (22). Whether this effect related to the long operation of stack F2 under higher current densities, which could be favorable for the Crdeposition due to decreased local oxygen partial as proposed by Menzler et al. (19) and Beez et al. (28), requires further investigation. In general, the observed Cr-amounts in the stacks with the MCF coating are low for both the LSCF and LSC electrodes. SEM and EDS analyses were performed, but no Cr could be identified within the electrodes due to the low amount.

TABLE II. Comparison of the Cr-amount in the air electrode following operation in the F-design stacks at \sim 700 °C

| t / h | Cr _{min} / μg·cm ⁻² | Cr _{max} / μg·cm ⁻² | Comments | Reference |
|----------|---|---|---------------------------|-------------------|
| ~2,500 | 22 | 71 | 700°C: 1,300 h | (19, 29) |
| | | | 600°C: 1,200 h | |
| ~7,500 | 33 | 105 | ~2,500 h with ambient air | Current work (F1) |
| ~13,000 | 13 | 26 | LSC electrode; | Current work (F2) |
| | | | Higher current | |
| ~35,000 | 4 | 8 | _ | (22) |
| ~100,000 | 291 | 517 | ITM interconnector, | (30) |
| | | | No MCF coating | |

Stacks in Cassette-design

Figure 3 shows the voltage evolutions of the two cassette-design stacks C1 (with LSCF) and C2 (with LSC). Unlike the two F-design stacks, the MCF coating was applied by means of WPS. In stack C1, there was no MCF coating in layers 11–17 (marked as blue lines in Figure 3) at all. Those interconnectors were only coated with a perovskite contact layer, which may also serve as a Cr-getter to a certain extent. The following information can be derived from Figure 3:

- Stack C1, operated near 785 °C, exhibited a relatively higher degradation rate from the beginning of its operation. All layers without MCF coatings featured poorer performance and slightly faster degradation compared to those with an MCF coating. The degradation rates slightly decreased after the first ~1,000 h of operation, and then became nearly constant for the layers with an MCF coating. The calculated voltage degradation up until 4,000 h was 0.8%kh⁻¹. The layers without the MCF coating initially showed essentially similar behavior, but with a higher degradation rate of 1.4%kh⁻¹ until ~2,500 h. After that, the degradation was further accelerated. Such fast degradation was initially assumed to be due to the difference in the coating. It turned out later that this could be caused by the degradation of layer 10 (marked as cyan in Figure 3). Starting from ~2,500 h, layer 10 degraded faster and was broken down later, after ~4,000 h. As a result of the severe leakage in this layer, all of the layers above layer 10 suffered from growing fuel utilization. Therefore, the analysis of the Cr-poisoning effect should focus more on the layers with MCF coatings.
- Apart from some small deviations in the cell voltages after several unexpected load interruptions, stack C2, when operated close to 737 °C, was very stable throughout the entire operation. It was operated under load for more than 11,000 h with a very low voltage degradation rate of 0.2%kh⁻¹.

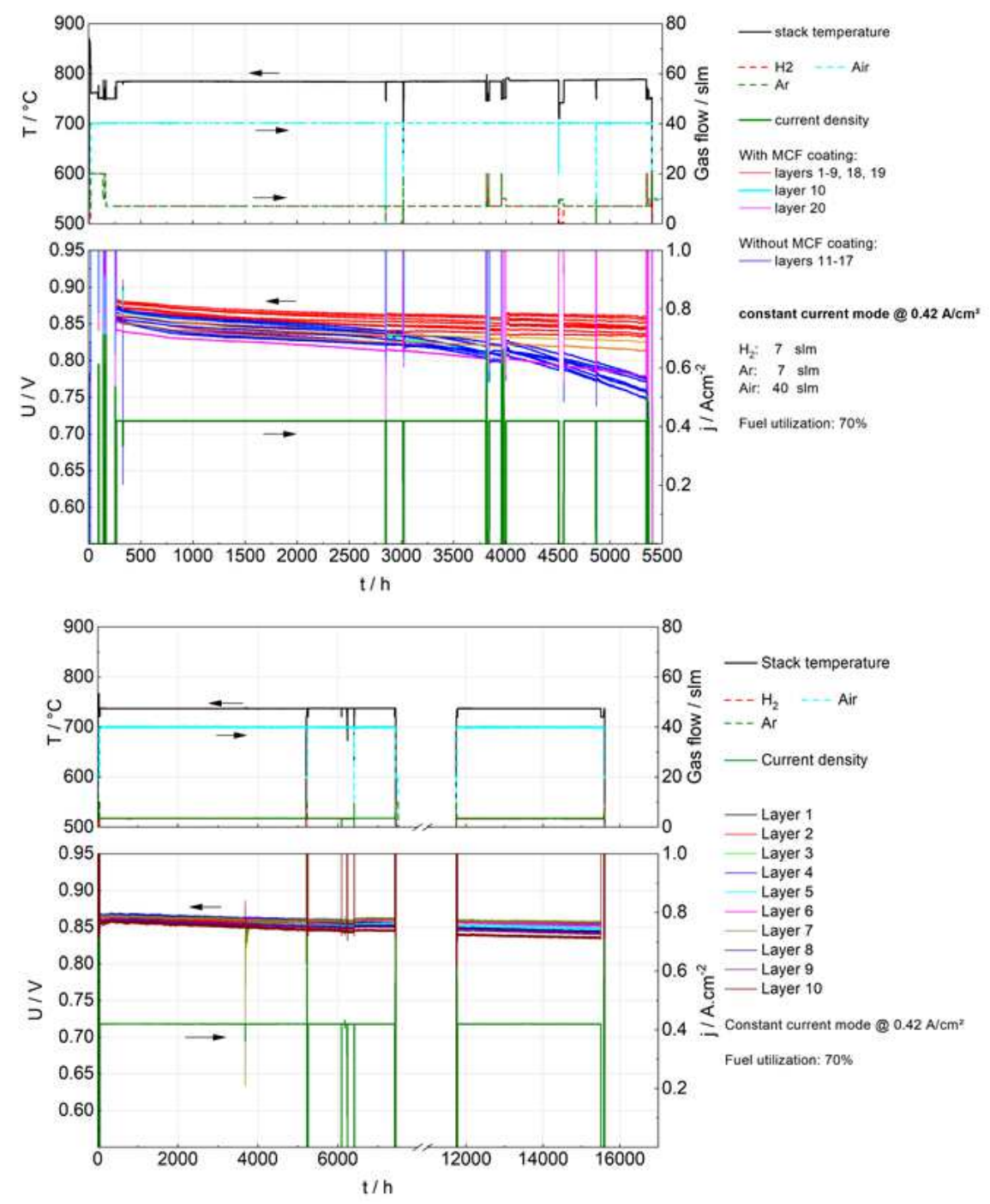


Figure 3. Two SOFC stacks in the cassette-design: (Top) stack C1 with an LSCF air electrode; and (bottom) stack C2 with an LSC air electrode. Note the different working temperatures and the difference in electrolyte thicknesses.

The EIS and DRT analyses, as shown in Figure 4, indicate noticeable degradation in both the air and fuel electrodes in stack C1 after ~3,500 h of operation. Moreover, the ohmic resistance was also increased. The degradation of the air electrode polarization and ohmic resistance could be explained by Cr-related mechanisms. However, the degradation at the fuel electrode following a relatively short operating period was not expected under the current testing conditions. Compared to stack C1, C2 showed only minimal changes in fuel electrode polarization after ~3,700 h of operation. Similar to the

F-design stacks with the APS-MCF shown in Figure 2, no modification in the air electrode polarization in stack C2 was visible, even with the WPS MCF coating.

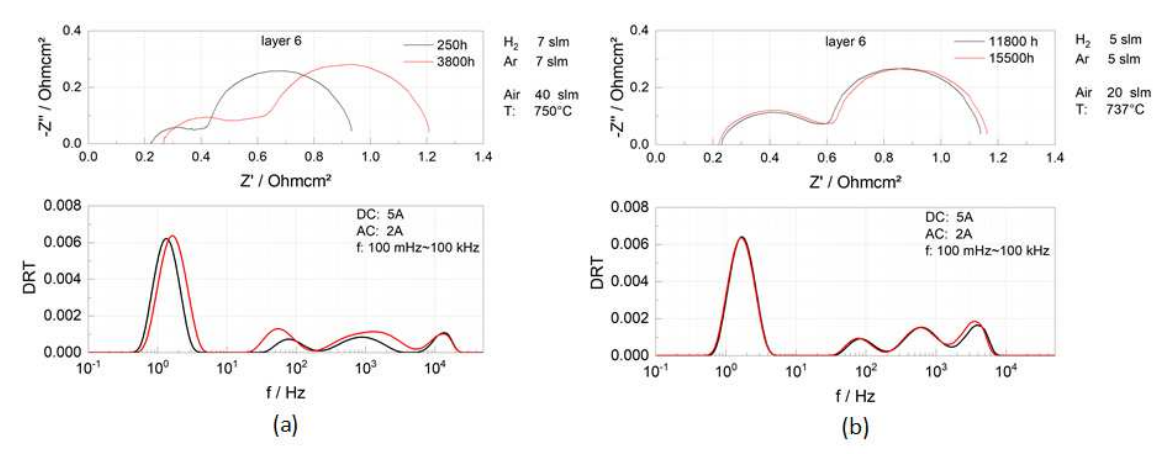


Figure 4. EIS and DRT analyses of cassette-design (a) stack C1 with the LSCF electrode; and (b) stack C2 with the thinner electrolyte and LSC electrode. From each stack, only layer 6 (with the WPS-MCF coating) is plotted. Note the slight difference in the temperature and testing periods.

TABLE III. Comparison of the Cr-amount in air electrode after operation in the cassette-design stacks

| | t / h | Cr _{min} / μg·cm ⁻² | Cr _{max} / μg·cm ⁻² | Comments |
|-------------------------|---------|---|---|---------------------|
| C1_without MCF | ~5,000 | | 96 | LSCF |
| C ₁ with MCF | ~5,000 | 41 | 49 | LSCF |
| C2 with MCF | ~11,000 | 31 | 34 | LSC, |
| _ | | | | thinner electrolyte |

The amounts of chromium incorporated on the air side in stacks C1 and C2 were analyzed by means of ICP-OES, and are listed in Table III. Similarly to the results in Table II, the Cr-amount is lower for the LSC electrode in stack C1, although the operating period was nearly doubled.

Again, no chromium could be identified within the electrodes on the basis of the SEM and EDS analyses. However, chromium could be found in both stacks, either inside the MCF coating applied by the WPS or on top of the contact layer. Figures 5 and 6 show the observed chromium in stacks C1 and C2, respectively. In Figure 5, chromium can be found in the rest MCF coating on top of the perovskite contact layer in stack C1. Inside the contact layer, no chromium is observed. In Figure 6, Cr-containing crystals can be found on top of the perovskite contact layer in stack C2.

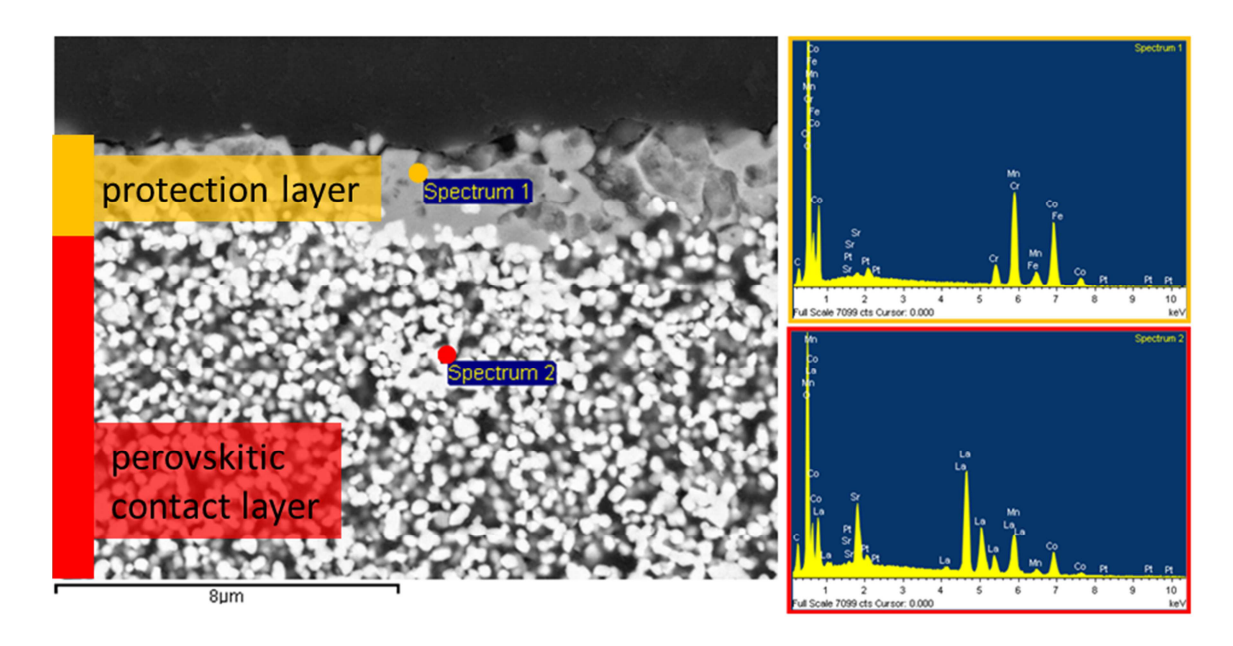


Figure 5. Chromium could be found within the rest MCF coating on top of the perovskitic contact layer in stack C1.

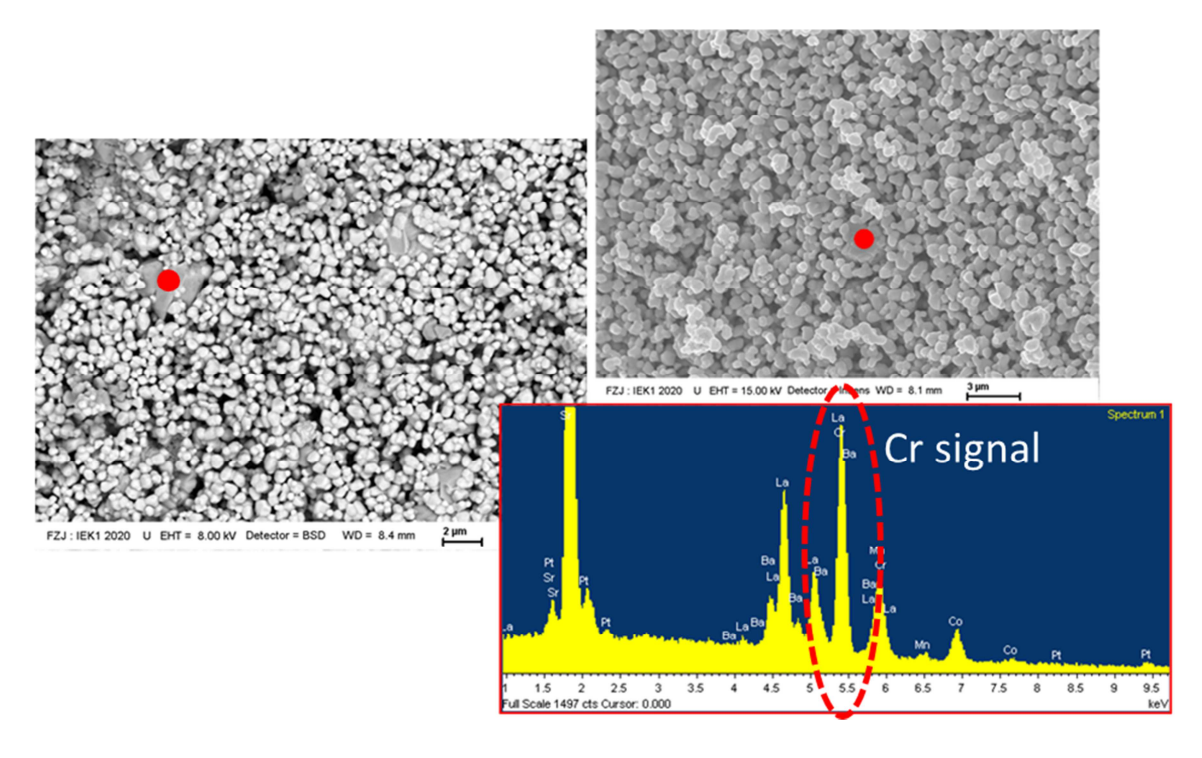


Figure 6. Chromium-containing crystals could be found on top of the perovskitic contact layer in stack C2.

The difference in chromium in Figures 5 and 6 could be explained by reference to the getter function of the porous MCF prepared by WPS. As can be seen in Figure 7, the WPS-MCF is porous and only has a thickness of $10\sim20~\mu m$. The thin and porous MCF is not sufficient to block the transport of chromium, but may only serve as a Cr-getter. Depending on the operating period, chromium may then proceed through the MCF and accumulate as isolated (Mn, Co, Fe, Cr) mixed oxide at the interface of the MCF and contact layer. For this reason, little chromium could be observed inside the air electrodes.

Based on this assumption, it can be expected that the cells may degrade faster once the interfacial resistance is dominated by the continuous growth of (Mn, Co, Fe, Cr) mixed oxide in the course of further operation.

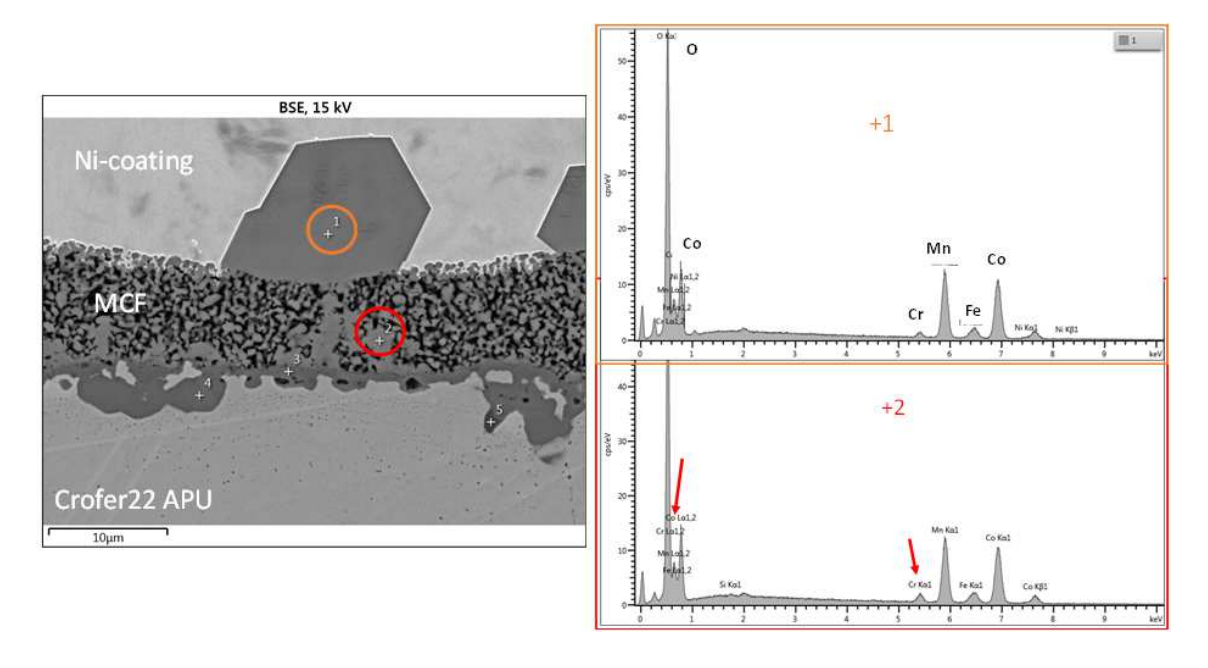


Figure 7. Porous MCF coating prepared by means of WPS and the incorporation of Cr inside the MCF in stack C2. (Courtesy of drs. Joanna Zurek and Dmitry Naumenko, IEK-2, Forschungszentrum Jülich GmbH)

Conclusions

In this study, Ni/YSZ-based ASCs with LSCF and LSC air electrodes from different suppliers were tested in two F-design and two cassette-design SOFC stacks, with the aim of investigating possibly differing degradation behaviors against Cr-poisoning. Stacks of the same design were tested in a similar manner for comparison. However, an exact comparison is not possible, as the testing conditions were not exactly identical. Therefore, the comparison of the results among different stacks should be considered qualitative rather than quantitative.

The stacks were tested with dry hydrogen as the fuel in the temperature range of 725–785°C for at least 5,000 hours. Compressed air was used in most cases, whereas one F-design stack with an LSCF was also partially tested with ambient air. The effect of ambient air on the degradation of the electrochemical performance was not observed across the testing period of over 1,000 hours. However, a possible acceleration effect on Cr-evaporation cannot be excluded yet, as the highest Cr-amount in the air electrode was measured among four stacks.

With an APS-MCF coating in F-design stacks, no Cr could be identified with SEM/EDS inside the electrodes and contact layer. The stack operated at a higher current density of 1 A·cm⁻² exhibited a slightly higher Cr-amount in the air electrode compared to an old stack, which was operated with 0.5 A·cm⁻² for \sim 30,000 hours. This may support the theory that the formation of SrCr_xO_y at the LSCF/GDC or LSC/GDC interface is

strongly dependent on the local Cr partial pressure and local oxygen partial pressure (28), which depend on the current densities.

In the case of the WPS-MCF coating in the cassette-design stacks, the MCF coating was thin and porous, and could only serve as a Cr-getter but not as a retention layer. Depending on the operating period, Cr could initially be accumulated within the MCF and later at the interface between the MCF and contact layer as an isolated (Mn, Co, Fe, Cr) mixed oxide. In the tested cassette-design stacks, chromium was only observed either on top of the contact layer or inside the MCF, but not inside the contact layer or electrode, even after more than 11,000 hours of operation. In this case, possible difference in the microstructural morphology between the LSCF and LSC caused by Cr-poisoning could not be revealed by SEM/EDS.

With respect to the possible higher resistance of LSC against Cr-poisoning, even though a thorough analysis of the morphology of an LSCF and LSC is not yet available, the following can be summarized on the basis of the long-term tests conducted:

- In both stack designs, the stack with LSC cells exhibited more stable performance than that with LSCF cells under the current testing conditions.
- Less Cr-content was measured in the LSC cells, despite the longer operating period.
- With the porous MCF prepared by WPS, the LSCF cells exhibited degradation in the air electrode that was not observed with LSC cells.

All of these results suggest a higher stability of LSC against Cr-deposition and Cr-poisoning, and more extensive and systematic studies are required to understand the mechanisms. For that, it is conceivable to compare and investigate the degradation of LSCF and LSC in further stacks tests without MCF coatings as a form of acceleration testing.

Acknowledgments

The authors would like to thank Ms. Ute de Haart for conducting the stack tests, Dr. Carole Babelot of the ZEA-1 for organizing the post-mortem analysis, Dr. Doris Sebold from the IEK-1 for the SEM operation of the cells, and drs. Joanna Zurek and Dmitry Naumenko from the IEK-2 for the SEM operation of the interconnector and protective coatings.

References

- 1. T. Horita, Ceram. Int., 47, 7293 (2021).
- 2. C. M. Harrison, P. R. Slater, and R. Steinberger-Wilckens, *Solid State Ionics*, **354**, 115410 (2020).
- 3. L. Zhou, J. H. Mason, W. Li, and X. Liu, *Renewable and Sustainable Energy Reviews*, **134**, 110320 (2020).

- 4. Z. Yang, M. Guo, N. Wang, C. Ma, J. Wang, and M. Han, *Int. J. Hydrogen Energy*, **42**, 24948 (2017).
- 5. S. P. Jiang and X. Chen, *Int. J. Hydrogen Energy*, **39**, 505 (2014).
- 6. J. W. Fergus, *Int. J. Hydrogen Energy*, **32**, 3664 (2007).
- 7. N. H. Menzler, A. Mai, and D. Stöver, in *Handbook of Fuel Cells*, A. L. W. Vielstich, H.A. Gasteiger, and H. Yokokawa, Editors, Vol. 5 Chapter 38, p. 1, John Wiley & Sons, Ltd. (2010).
- 8. S. P. Jiang and Y. Zhen, *Solid State Ionics*, **179**, 1459 (2008).
- 9. N. Shaigan, W. Qu, D. G. Ivey, and W. Chen, *J. Power Sources*, **195**, 1529 (2010).
- 10. R. Valssen, N. Grunwald, D. Marcano, N. H. Menzler, R. Mucke, D. Sebold, Y. J. Sohn, and O. Guillon, *Surf. Coat Tech.*, **291**, 115 (2016).
- 11. N. Grünwald, P. Lhuissier, L. Salvo, J. Villanova, N. H. Menzler, O. Guillon, C. L. Martin, and R. Vaßen, *J. Mater. Sci.*, **55**, 12725 (2020).
- 12. L. Blum, U. Packbier, I. C. Vinke, and L. G. J. de Haart, *Fuel Cells*, **13**, 646 (2013).
- 13. S. M. Gross-Barsnick, Q. Fang, P. Batfalsky, L. Niewolak, L. Blum, and W. J. Quadakkers, *Fuel Cells*, **19**, 84 (2019).
- 14. L. Blum, Q. Fang, S. M. Groß-Barsnick, L. G. J. de Haart, J. Malzbender, N. H. Menzler, and W. J. Quadakkers, *Int. J. Hydrogen Energy*, **45**, 8955 (2020).
- 15. Q. P. Fang, L. Blum, P. Batfalsky, N. H. Menzler, U. Packbier, and D. Stolten, *Int. J. Hydrogen Energy*, **38**, 16344 (2013).
- 16. H. Yokokawa, T. Horita, N. Sakai, K. Yamaji, M. E. Brito, Y. P. Xiong, and H. Kishimoto, *Solid State Ionics*, **177**, 3193 (2006).
- 17. E. Bucher, M. Yang, and W. Sitte, *J. Electrochem. Soc.*, **159**, B592 (2012).
- 18. E. Bucher, C. Gspan, T. Höschen, F. Hofer, and W. Sitte, *Solid State Ionics*, **299**, 26 (2017).
- 19. N. H. Menzler, D. Sebold, and Q. P. Fang, *J. Electrochem. Soc.*, **162**, F1275 (2015).
- 20. Q. P. Fang, L. Blum, R. Peters, M. Peksen, P. Batfalsky, and D. Stolten, *Int. J. Hydrogen Energy*, **40**, 1128 (2015).
- 21. T. H. Wan, M. Saccoccio, C. Chen, and F. Ciucci, *Electrochim. Acta*, **184**, 483 (2015).
- 22. N. H. Menzler, D. Sebold, and O. Guillon, *J. Power Sources*, **374**, 69 (2018).
- 23. M. Lang, C. Bohn, M. Henke, G. Schiller, C. Willich, and F. Hauler, J. Electrochem. Soc., 164, F1460 (2017).
- 24. Q. Fang, U. de Haart, D. Schäfer, F. Thaler, V. Rangel-Hernandez, R. Peters, and L. Blum, *J. Electrochem. Soc.*, **167**, 144508 (2020).
- 25. A. Leonide, B. Ruger, A. Weber, W. A. Meulenberg, and E. Ivers-Tiffee, *Solid Oxide Fuel Cells 11 (Sofc-Xi)*, **25**, 2487 (2009).
- 26. Y. Yan, Q. Fang, L. Blum, and W. Lehnert, *Electrochim. Acta*, **258**, 1254 (2017).
- 27. Q. P. Fang, L. Blum, and D. Stolten, *J. Electrochem. Soc.*, **166**, F1320 (2019).
- 28. A. Beez, X. Yin, N. H. Menzler, R. Spatschek, and M. Bram, *J. Electrochem. Soc.*, **164**, F3028 (2017).
- 29. N. H. Menzler, D. Sebold, and E. Wessel, *J. Power Sources*, **254**, 148 (2014).
- 30. N. H. Menzler, D. Sebold, Y. J. Sohn, and S. Zischke, *J. Power Sources*, **478**, 228770 (2020).